# Features of ecological half-lives of air dose rate reduction in Fukushima clarified by least absolute shrinkage and selection operator regression analysis

Kimiaki SAITO[a], Yoshiaki SHIKAZE[a], Naoki TANIMURA[b],
Kazuya YOSHIMURA[c], Liu XUDONG[a], Masahiko MACHIDA[a]

[a] Japan Atomic Energy Agency, 178-4-4 Wakashiba, Kashiwa, Chiba 227-0871, Japan
[b] Mizuho Research & Technologies, Ltd., 2-3 Kanda-Nishikicho, Chiyoda-ku, Tokyo 101-8443, Japan
[c] Japan Atomic Energy Agency, 45-169 Sukakeba, Kaihama, Haramachi-ku, Minamisoma 975-0036, Japan.

*Corresponding author
Kimiaki Saito
address: 178-4-4 Wakashiba, Kashiwa, Chiba 227-0871, Japan
phone: ++81 80 9771 0741,
e-mail: saito.kimiaki@jaea.go.jp

**Author contribution**

**K. Saito**: Project administration, Conceptualization, Writing **Y. Shikaze**: Formal analysis **N. Tanimura**: Investigation **K. Yoshimura**: Funding acquisition, Supervision **L. Xudong**: Methodology **M. Machida**: Supervision, Project administration

# Features of ecological half-lives of air dose rate reduction in Fukushima clarified by least absolute shrinkage and selection operator regression analysis


## Abstract

The two-component model with a fast-decay and a slow-decay component has been widely used to approximate the decreasing trend of air dose rates in contaminated areas. The adequacy of the two-component model is yet to be thoroughly validated. This study analyzed many car-borne survey data obtained after the Fukushima Daiichi Nuclear Power Plant accident from 2011 to 2016 using the least absolute shrinkage and selection operator regression with a high degree-of-freedom model to investigate the adequacy of the two-component model and the profiles of ecological half-lives. The results show that the two-component model can approximate the decreasing trend of air dose rates in the Fukushima area well in most cases. However, in approximately 20% of the cases, the one-component model can approximate the trend better. The fast-decay component in the two-component model has a sharp ecological half-life peak at less than 1 y, with a frequency distribution peaking at 0.3–0.4 y. However, in approximately half of the cases, the slow-decay component has a broad half-life peak with a frequency distribution covering several years to over 50 y. The reduction speed of the air dose rate was fast in the order of urban areas, paddy fields, croplands, deciduous forests, and evergreen forests and became slow as the initial air dose rate increased, which is explained by the weight given for the fast-decay component rather than the value of ecological half-life.



**Keywords:** Fukushima accident, air dose rate, car-borne survey, LASSO regression analysis, two-component model, ecological half-life

## 1. Introduction

The Fukushima Daiichi Nuclear Power Plant accident (Fukushima accident) in 2011 caused the deposition of large amount of released anthropogenic radionuclides over vast areas in Japan, significantly increasing environmental radiation levels (IAEA 2015). The radiation levels in the areas affected by the Fukushima accident have decreased with elapsed time, whereas the radiation levels in some areas are expected to remain high for a long time because of the long half-lives of radioactive cesium, mostly $^{137}Cs$. Understanding the decreasing trend of radiation levels is essential for taking optimum measures for radiation protection, environmental remediation, social restoration, and future accident preparation.

After the Fukushima accident, many organizations performed numerous environmental monitoring activities, and an enormous amount of monitoring data has been accumulated (Saito and Onda, 2015; Sanada et al., 2014; Fukushima Prefecture, 2024; MAFF, 2014). The monitoring activities initiated by the Ministry of Education, Culture, Sports, Science, and Technology and inherited by the Nuclear Regulatory Authority have provided critical monitoring data (Saito and Onda, 2015) because the environmental monitoring was conducted systematically using reliable monitoring methods. The obtained data are publicly available through the specified database (JAEA, 2024; Seki, 2021).

Multiple researchers have analyzed the decreasing trend of ambient dose equivalent rates (air dose rates) in terms of ecological half-lives (Gale et al., 1964; Kinase et al., 2014, 2017; Andoh et al., 2018a, 2018b; Sanada et al., 2018; Wainwright et al., 2018). The ecological half-lives should indicate the velocity of air dose-rate reduction according to radiocesium migration and not include the dose reduction of physical decay. In many cases, the two-component model was employed when determining the ecological half-lives, assuming that

50 the air dose rate will decrease according to two exponential functions with short and long
51 ecological half-lives.
52 The analyses after the Fukushima accident support the effectiveness of the two-
53 component model. The decreasing tendency is frequently well-fitted using two exponential
54 functions for different datasets. Most studies determined the short half-life to be less than
55 one year, whereas the long half-life varied widely from several years to several tens of years,
56 as summarized by Saito et al. (2019). It still needs to be thoroughly established if the two-
57 component model best fits the observed data. Therefore, it is worth examining how many
58 components are most suitable to fit the time series of monitoring data obtained after the
59 Fukushima accident and how the ecological half-live profile changes according to land use
60 and dose rate.
61 The least absolute shrinkage and selection operator (LASSO) regression analysis
62 (Tibshirani, 2011; Muthukrishnan and Rohini, 2016) with a model comprising many
63 exponential functions with different ecological half-lives was employed to investigate how
64 many components are most suitable for modeling the observed air dose rate trend. In the
65 general regression for observed data with uncertainties, too many parameters result in
66 overfitting, where the regression curve follows the fluctuated data excessively. LASSO
67 analysis avoids overfitting by adding an L1 regulation term to the loss function. This method
68 can determine the optimal number of basis functions and the parameters.
69 The purpose of this study was to examine the optimal number of components in the trend
70 model for approximating the temporal change of air dose rates observed after the Fukushima
71 accident and to clarify the characteristics of ecological half-lives. Therefore, LASSO
72 regression analysis was applied to big car-borne survey data obtained after the Fukushima
73 accident (Andoh et al., 2015; 2018b).
74

## 2. Materials and methods

### 2.1 Air dose rate data

The air dose rate data for the LASSO analysis were required to satisfy several fundamental conditions. The measurements must have started in the early phase after the accident. The data must have been obtained regularly with a specific frequency to follow the temporal trend appropriately. The measurements needed to have been performed over wide areas covering diverse conditions, such as different land uses, geological regions, and air dose rate levels, resulting in sufficient air dose rate data suitable for statistical analysis. Furthermore, the reliability and accuracy of the measurements are essential.

Considering these requirements, the car-borne surveys conducted in the Fukushima mapping project were selected (Andoh et al., 2015; 2018b). In the Fukushima mapping project, the air dose rates have been obtained using four methods. Among them, car-borne surveys have accumulated enormous air dose rate data. The first survey was launched in June 2011, and the surveys were performed twice a year. The car-borne surveys covered wide areas in eastern Japan (Ando et al., 2015; 2018b) employing the Kyoto University RAdiation MApping (KURAMA) system (Tanigaki et al., 2013; 2015).

The measurement performance of the system was evaluated using a standard irradiation facility for gamma energy, dose rate, and directional responses (Tsuda et al., 2015) to certify that the performance is subject to the Japan Industrial Standard (JIS) Z4333, the authorized standards for commercially available survey meters in Japan (JIS, 2006). Andoh et al. evaluated the overall uncertainty of the car-borne measurements using the KURAMA-II system as 15% (2015). In the mapping project, the car-borne survey data were averaged in a $100 \times 100$ m$^2$ area to reduce the statistical fluctuation. Therefore, we analyzed the temporal change in the average air dose rate within each $100 \times 100$ m$^2$ pixel.

99 The analysis used the car survey data obtained in Fukushima prefecture from the first (June
100 2011) to the thirteenth (December 2016) campaigns. The period of the analyzed data was
101 selected so that it does not significantly differ from those in past studies to compare the
102 obtained results in similar conditions. Table 1 outlines the 13 car-borne survey campaigns.
103 The middle day of each campaign period was taken to be the measurement day for all data
104 obtained. The uncertainty in the measurement day was a month at maximum, which is
105 considered negligible compared to other uncertainties. The elapsed time after the accident was
106 calculated from the midday of March 15, 2011. The following analysis was performed for the
107 pixels with more than 11 data in the 13 campaigns. In other words, the pixel was not used in
108 the analysis if the number of missing data within the 13 campaigns was zero or one. The total
109 number of data to fulfill this condition was 21,341.
110 If a missing datum exists in a series of air dose rates, it is complemented using the random
111 forest method (Breiman, 2001; Stekhoven and Bühlmann, 2012). The missing data can be
112 estimated by learning from data at other locations where information is available or by
113 learning from data at different time points at the same location. In this case, the former
114 approach was more appropriate. Therefore, using the model based on learning from other
115 locations, we applied random forest to the reference data from multiple locations and
116 estimated the missing values to create a complete dataset without any missing.
117
118 2.1 LASSO analysis
119 In the LASSO analysis, the decreasing tendency of observed air dose rates at each pixel
120 was fitted using a linear combination model of an arbitrary number of exponential functions
121 with different ecological half-lives, and the optimal parameters were determined. The
122 following equation was employed for the fitting.

$$D(t) = c_0 + \frac{k\exp(-\lambda_{134}t) + \exp(-\lambda_{137}t)}{k+1} \sum_{i=1}^{N_e} c_i \exp(-\lambda_i t) \quad (1)$$

where

$D(t)$: the air dose rate at time $t$ (μSv/h),

$k$: the ratio of the air dose rate between $^{134}$Cs and $^{137}$Cs at $t = 0$,

$\lambda_{134}$ and $\lambda_{137}$: the radioactive decay constants of $^{134}$Cs and $^{137}$Cs ($y^{-1}$), respectively,

$N_e$: the number of assumed basis functions,

$\exp(-\lambda_i t)$: the basis function,

$\lambda_i$: the attenuation constant depending on each ecological half-life ($y^{-1}$),

$c_i$: the coefficient of each basis function (μSv/h).

In this study, *Ne* was 50, and the 50 exponential functions with different attenuation constants were used. Here, $c_0$ corresponds to the background radiation level of each location, and $c_i$ was assumed never to be negative (nonnegative LASSO). The ecological half-life $t_{1/2}$ is related to the attenuation constant $\lambda$ by $\ln 2/t_{1/2} = \lambda$.

The optimal combination of $c_i$ was determined so that the following objective function becomes minimum.

$$f(\boldsymbol{C}) = \frac{1}{N_t} \sum_{s=1}^{N_t} (D_m(t_s) - D(t_s))^2 + \alpha \|\boldsymbol{C}\|_1 \quad (2)$$

where

$\boldsymbol{C}$: the vector representation for $c_1, \ldots, c_{Ne}$,

$N_t$: the number of sequential data,

$D_m(t_s)$: the observed air dose rate at $t_s$,

$\alpha$: the L1 norm coefficient.

$N_t$ was 13. The L1 norm term added to the objective function prevents selecting excessive exponential functions. The LASSO analysis results depend on the value of $\alpha$; the larger $\alpha$ tends to select a smaller number of exponential functions. This study determined the $\alpha$ value objectively using a cross-validation method.

The L1 norm coefficient, called the hyperparameter $\alpha$ in LASSO, can be optimized using cross-validation. In the validation scheme, the input data are divided into k-fold groups, and one of the groups is chosen and used as the test data. Then, LASSO is applied using the remaining k-1 group as the training data. Since k-1 LASSO solutions can be obtained for each $\alpha$, the error evaluation is performed on the test data, and $\alpha$ can be optimized (Shi et al., 2023). In this study, k was taken to be five.

The shortest and longest ecological half-lives were assumed to be 0.1 y and 50 y, respectively, considering the results of past studies. Then, the ecological attenuation coefficients $\lambda_i$ were given to cover the tendencies of air dose rate attenuation evenly between those for half-lives of 0.1 y and 50 y (Fig. 1). Table 2 lists the ecological half-lives corresponding to these $\lambda_i$.

## 3. Results and discussion

A set of $c_i$ was determined for each of the targeted 21,341 pixels classified by land-use categories according to the Japan Aerospace Exploration Agency's (JAXA's) data Ver. 14.2 (JAXA, 2014): water, urban, paddy, crop, grass, deciduous forest, evergreen forest, and bare surface. The following discussion addresses the five dominant land-use categories of urban, paddy, crop, deciduous forest, and evergreen forest because each has sufficient pixels to analyze statistically.

Furthermore, the pixels whose initial air dose rates in June 2011 were greater than 0.2 μSv/h were selected. It was judged that the decreasing tendency of air dose rates due to radiocesium would be challenging to analyze properly for pixels with initial air dose rates less than 0.2 μSv/h because the radiation levels were comparable to the background air dose rates evaluated from car-borne survey data (Andoh, et al., 2017). Table 3 shows the number of pixels belonging to the five dominant categories. The total number of pixels analyzed after the selection due to the initial dose rate was 18,694.

Figure 2 shows some examples of the decreasing trend of air dose rates calculated by Equation 1), with the determined parameters and the observed air dose rates. It is recognized that the LASSO analysis likely reconstructed the decreasing tendency.

### 3.1 Model component features

The number of components adequately representing the decreasing trend of the air dose rate was examined based on the LASSO analysis results. Here, we established the following rule to count the component number. If nonzero $c_i$'s were determined sequentially, they were recognized as one component. For example, if nonzero values were given for $c_{11}$, $c_{12}$, and $c_{13}$, the series of these coefficients was counted to be one component. In this analysis, the 50 discrete ecological half-lives were prepared; then, if the actual ecological half-live exists between two prepared half-lives, it is natural that the $c_i$'s are determined for the two exponential functions with the half-lives existing on both sides of the actual half-life. Furthermore, radiocesium migration in the real environment is complex, and it is inferred that some radiocesium groups have similar migration characteristics. These groups are difficult to analyze separately and cannot avoid classifying into the same component.

The number of components representing the trend was within three for all cases. Table 4 lists the proportion of the component numbers of the selected models for the five land-use

categories. The difference due to land use was insignificant. The proportion of the three-component model was less than 1% for any land-use category. In approximately 80% of cases, the two-component model was selected, and in approximately 20%, the one-component model. This result indicates that the two-component model, which has been employed widely, would be an appropriate approximation for representing the radiation level trend in most cases.

Next, we examined how many exponential functions constitute each component of the models. Figures 3 and 4 give the statistics on the number of exponential functions constituting the two-component and one-component models, respectively. The fast-decay component of the two-component model has a sharp peak in terms of ecological half-life; the cases where the number of exponential functions is one or two occupied more than 90% of the total cases, and those where the number is one to three is approximately 98%. Thus, a single value or a narrow half-width peak represented the ecological half-life of the fast-decay component.

The slow-decay component of the two-component model indicated different features. Approximately 50% of the slow-decay component was expressed by one exponential function, whereas the other 50% comprised plural exponential functions rather evenly distributed up to 20 functions. The former cases include the ecological half-life determined to be 50 y. In these cases, the actual half-life can have widths of more than 50 y. Therefore, most ecological half-lives of the slow-decay component have some widths.

For the one-component model, two or three exponential functions are most probable, and 80% of the one-component model has less than seven basis functions, whereas the rest have basis functions distributed up to 25 functions. The half-lives of the one-component model were more than 1 y, corresponding to the slow-decay component of the two-component model.

The reasons for the specific features described above are unclear and remain future challenges to be clarified. However, it is speculated that the targeted period of five years after the accident was long enough to determine the exact half-life of the fast-decay component, which is mostly smaller than one year. However, it is too short to determine the half-life of the slow-decay component, which covers wide periods up to several tens of years.

Another possibility would be that radiocesium deposited on artificial surfaces, such as roads, parking places, and the roofs and walls of houses, is removed shortly after deposition, leading to an apparent similar short half-life after deposition. However, radiocesium with long ecological half-lives might include those with different migration properties. Radiocesium deposited on the ground penetrates the ground gradually, leading to a steady dose rate reduction due to the increment in the gamma-ray shielding effect. A small portion of radiocesium migrates horizontally, resulting in a further reduction in air dose rates. Human activities, such as cultivation, accelerate radiocesium migration. These radiocesium movements could be represented by a half-life peak with a broad width.

### 3.2 Average profile of ecological half-lives

The characteristics of the average profiles of ecological half-lives were investigated by normalizing a set of $c_1$ to $c_{50}$ to their sum because their absolute values change with the radiation level. We would like to evaluate the relative relations among the coefficients. Next, each coefficient was averaged over whole pixels belonging to the same land-use category where the initial air dose rates were more than 0.2 μSv/h.

Figure 5 shows the average profiles of normalized coefficients of basis functions with different ecological half-lives for five land-use categories. The profile has a clear peak below a half-life of 1 y, corresponding to the fast-decay component regardless of land use. Furthermore, the profile shows a low and wide hump over a wide half-life range from 1 to

more than 10 years, corresponding to the slow-decay component. The coefficient $c_{50}$, which corresponds to a half-life of 50 y, has a specific value, even though it is not indicated in the figure. The peak height for the fast-decay component differs according to land use: high for urban, low for evergreen forests, and in between for the others. However, the position and shape of the peak do not differ according to land use. The average normalized coefficient values were summed over half-life ranges of less than 1 y and more than 1 y (Table 5).

The difference in the summed values of the coefficients is related to the variations in the dose rate reduction tendency. Figure 6 shows the decreasing tendency of air dose rates during the two years after the accident for different land uses. The fundamental features concerning land-use dependency are similar to those found in previous studies on car-borne survey data (Kinase et al., 2017; Andoh et al., 2018b). The decrease in air dose rates is fast in the order of urban, crop, paddy, deciduous forest, and evergreen forest, which is in the same order as the summed values of the coefficients below a half-life of 1 y. Therefore, the speed of the air dose rate reduction in the early stage is related to the weight (summed coefficients) given to the exponential functions with ecological half-lives below 1 y but not to the average value of the ecological half-life indicated in Table 6.

The mobility of radiocesium in the environment has explained the difference in the dose rate reduction. Radiocesium deposited on artificial structures, such as paved roads, paved parking places, and the walls and roofs of houses, is removed and washed off quickly after deposition (Yoshimura et al., 2017), leading to a fast air dose rate reduction. However, radiocesium deposited in forests moves slowly within the forest system (Kato et al., 2018a; Takahashi, 2018), and the discharge rate from the forest system is very small (Funaki et al., 2018). Consequently, the dose rate reduction in forests is generally slow. The air dose rate in evergreen forests was slower than that in deciduous forests, coinciding with the direct observation of air dose rates in forests (Kato et al., 2018b).

Since car-borne surveys were performed on paved roads where deposited radiocesium is removed quickly, the survey data show a faster reduction tendency than those measured on undisturbed fields. However, gamma rays from the surrounding environments outside of roads are also detected in car-borne surveys. Therefore, car-borne survey data reflect the air dose rate reduction tendency depending on land use.

To clarify the dose rate dependency of air dose rate reduction, the profiles of ecological half-lives were classified according to the initial air dose rate ranges in June 2011: 1) 0.2–0.5 μSv/h, 2) 0.5–1.0 μSv/h, 3) 1.0–1.9 μS/h, and 4) more than 1.9 μSv/h.

Figure 7 shows the average profiles of ecological half-lives classified by the four initial dose rate ranges for evergreen forest, paddy, and urban. The three typical land-use categories were selected to avoid confusion by plotting too much data. The weights given to the fast-decay component decrease with the increasing initial air dose rate. Consequently, the weights given to the slow-decay components increase. Concerning the slow-decay component in high dose rate ranges, especially more than 1.9 μSv/h, a clear peak is observed around the ecological half-lives of several years.

Figure 8 shows the decreasing tendency of air dose rates classified by the initial dose rate ranges. The decreasing tendency becomes slow as the initial air dose rate increases. The air dose rate decrease is noticeably slow above 1.9 μSv/h. This result can be explained by the weight proportions for the fast- and slow-decay components shown in Table 5. The larger the proportion for the fast-decay component, the faster the dose rate reduction. As the initial dose rate increases, the proportion of the fast-decay component weight decreases, resulting in a slower dose rate reduction. There were many human activities in the low-radiation areas even after the accident, whereas, in highly contaminated areas, inhabitant residence was restricted and human activities were scarce. Human activities including official and voluntary

293 decontamination tend to accelerate the air dose rate reduction (Saito et al., 2019), indicating
294 why the initial air dose level has a connection with the air dose rate reduction.
295 The average ecological half-lives for fast-decay and slow-decay components do not
296 change much (Table 6). The ecological half-life of 50 y was not included in the calculation of
297 the average half-life for the slow-decay component because the exponential function
298 represents an ecological half-life of 50 y and a wider range of ecological half-life of more
299 than 50 y. Most average half-lives for the fast-decay component fall between 0.3 y and 0.4 y,
300 regardless of the initial dose rate and land use. The average half-life for the slow-decay
301 component decreases slightly with the increasing initial dose rate; nevertheless, most average
302 half-lives exist between 5 y and 8 y.
303
304 **4. Conclusions**
305 A LASSO regression analysis applied to enormous car-borne survey data in Fukushima
306 clarified the features of air dose rate reduction trends after a large-scale nuclear accident. The
307 two-component model, which has been employed widely, approximated the decreasing trend
308 of air dose rates adequately in most cases. However, in some cases, the one-component model
309 can approximate the trend better. The fast-decay component of the two-component model has
310 a sharp peak of ecological half-life, and the frequency distribution peaks at 0.3−0.4 y.
311 However, about half of the slow-decay component has a wide half-life peak, expressed by
312 plural exponential functions. The half-life of the slow-decay component covered a wide
313 period from several years to several tens of years. The reduction speed of the air dose rate for
314 a few years after the accident is deeply related to the weight given to the fast-decay
315 component of the two-component model but not to the absolute value of the half-life. Air
316 dose rates have decreased faster in the order of urban, paddy, crop, deciduous forest, and
317 evergreen forest. The radiocesium migration properties in the environment can explain this

result. As the initial air dose rate increased, the reduction speed slowed. This study's results should provide basic information on modeling temporal changes in contamination conditions.

**Acknowledgements**

This study was supported by Research project on the Health Effects of Radiation organized by the Ministry of the Environment, Japan

**References**

Andoh, M., Nakahara, Y., Tsuda, S., Yoshida, T., Matsuda, N., Takahashi, F., Mikami, S., Kinouchi, N., Sato, T., Tanigaki, M., Takamiya, K., Sato, N., Okumura, R., Uchihori, Y., Saito, K., 2015. Measurement of air dose rates in wide area around the Fukushima Daiichi nuclear power plant through a series of car-borne surveys. J. Environ. Radioact. 139, 266-280.

Andoh, M., Matsuda, N., Saito, K., 2017. Evaluation of Ambient Dose Equivalent Rates Owing to Natural Radioactive Nuclides in Eastern Japan by Car-Borne Surveys Using KURAMA-II. (in Japanese) Transactions of the Atomic Energy Society of Japan. 16, 63-80.

Andoh, M., Mikami, S., Tsuda, S., Yoshida, T., Matsuda, N., Saito, K., 2018a. Measurement of air dose rates by walk survey around the Fukushima Dai-ichi Nuclear Power Plant using KURAMA-II until 2016. J. Environ. Radioact. 190-191, 111–121.

Andoh, M., Mikami, S., Tsuda, S., Yoshida, T., Matsuda, N., Saito, K., 2018b. Decreasing trend of ambient dose equivalent rates over a wide area in eastern Japan until 2016 evaluated by car-borne surveys using KURAMA Systems. J. Environ. Radioact. 192, 385–398.

Breiman, L., 2001. Random forests. Machine learning 45, 5-32.

Fukushima Prefecture, 2024. Fukushima Prefecture Environmental Radiation Monitoring-Mesh Investigation. https://www.pref.fukushima.lg.jp/site/portal/ps-monitaring-mesh.html, Accessed data: 6 March 2024.

Funaki, H., Yoshimura, K., Sakuma, K., Iri, S., Oda, Y., 2019. Evaluation of particulate $^{137}$Cs discharge from a mountainous forested catchment using reservoir sediments and sinking particles. J. Environ. Radioact. 210, 105814. https://doi.org/10.1016/j.jenvrad.2018.09.012

Gale, H.L., Humphreys, D.L.O., Fisher, E.M.R., 1964. Weathering of caesium-137 in soil. Nature 4916, 257–261.

IAEA (International Atomic Energy Agency), 2015. The Fukushima Daiichi Accident. ISBN:978-92-0-107015-9.

JAEA (Japan Atomic Energy Agency), 2024. Database for Radioactive Substance Monitoring Data. https://emdb.jaea.go.jp/emdb/ , Accessed date: 6 March 2024.

JAXA (Japan Aerospace Exploration Agency), 2014. High-Resolution Land-Use and Land-Cover Map. Ver 14.2. (provided by JAEA's HP)
https://emdb.jaea.go.jp/emdb_old/en/portals/2030101000/

JIS (Japanese Industrial Standards), 2006. Portable Photon Ambient Dose Equivalent Rate Meters for Use in Radiation Protection (Japanese). Japanese Standards Association, Japan.

Kato, K., Onda, Y., Saidin, Z.H., Sakashita, W., Hisadome, K., Loffredo, N., 2018a. Six-year monitoring study of radiocesium transfer in forest environments following the Fukushima nuclear power plant accident. J. Environ. Radioact. 210, 105817
https://doi.org/10.1016/j.jenvrad.2018.09.015

Kato, H., Onda, Y., Yamaguchi, T., 2018b. Temporal changes of the ambient dose rate in the forest environments of Fukushima Prefecture following the Fukushima reactor accident. J. Environ. Radioact. 93-94, 20-26.

Kinase, S., Sato, S., Takahashi, T., Sakamoto, R., Saito, K., 2014. Ecological Half-life of Radioactive Caesium within the 80 km Radius of the Fukushima Daiichi Nuclear Power Plant. IRPA2014 Abstract Book 163-166.

Kinase, S., Takahashi, T., Saito, K., 2017. Long-term prediction of ambient dose equivalent rates after the Fukushima Daiichi nuclear power plant accident. J. Nucl. Sci. Technol. 54, 1345-1354. DOI: 10.1080/00223131.2017.136565

MAFF (Ministry of Agriculture Forestry and Fisheries of Japan), 2014. Monitoring results of ambient dose rate in forest of Fukushima Prefecture (in Japanese). https://www.rinya.maff.go.jp/kanto/press/kikaku/140716.html, Accessed on March 2024.

Muthukrishnan, R., Rohini, R., 2016. LASSO: A feature selection technique in predictive modeling for machine learning. IEEE International Conference on Advances in Computer Applications (ICACA), Coimbatore, India, 2016, pp. 18-20.

Saito, K., Onda, Y., 2015. Outline of the national mapping projects implemented after the Fukushima accident. J. Environ. Radioact. 139, 240-249.

Saito, K., Mikami, S., Andoh, M., Matsuda, N., Kinase, S., Tsuda, S., Yoshida, T., Sato, T., Seki, A., Yamamoto, H., Sanada, Y., Wainwright-Murakami, H., Takemiya, H., 2019. Summary of temporal changes in air dose rates and radionuclide deposition densities in the 80 km zone over five years after the Fukushima Nuclear Power Plant accident. J. Environ. Radioact. 210, 105878 https://doi.org/10.1016/j.jenvrad.2018.12.020

Sanada, Y., Sugita, T., Nishizawa, Y., Kondo, A., Torii, T., 2014. The aerial radiation monitoring in Japan after the Fukushima Daiichi nuclear power plant accident. J. Prog. In Nucl. Sci. Technol. 4, 76-80.

Sanada, Y., Urabe, Y., Sasaki, M., Ochi, K., Torii, T., 2018. Evaluation of ecological half-life of dose rate based on airborne radiation monitoring following the Fukushima Daiichi nuclear plant accident. J. Environ. Radioact. 192, 417–425.

Seki, A., Saito, K., Takemiya, H., 2021. Current status of the environmental monitoring database on the accident at Fukushima Daiichi Nuclear Power Plant. J. Radiol. Prot. 41, S89-S98. https://doi.org/10.1088/1361-6498/abfbc1

Stekhoven, D.J., Bühlmann, P., 2012. MissForest—non-parametric missing value imputation for mixed-type data. Bioinformatics 28, 112-118.

Takahashi, J., Onda, Y., Hihara, D., Tamura, K., 2018. Six-year monitoring of the vertical distribution of radiocesium in three forest soils after the Fukushima Dai-ichi Nuclear Power Plant accident. J. Environ. Radioact. 210, 105811 https://doi.org/10.1016/j.jenvrad.2018.09.009

Tanigaki, M., Okumura, R., Takamiya, K., Sato, N., Yoshino, H., Yamana, H., 2013. Development of a car-borne g-ray survey system, KURAMA. Nucl. Instr. Meth. Phys. Res. Sec. A 726, 162-168.

Tanigaki, M., Okumura, R., Takamiya, K., Sato, N., Yoshino, H., Yoshinaga, H., Kobayashi, Y., Uehara, A., Yamana, H., 2015. Development of KURAMA-II and its operation in Fukushima. Nucl. Instrum. Meth. Phys. Res. 781, 57–64.

Tibshirani, R., 2011. Regression shrinkage and selection via the lasso: a retrospective. Journal of the Royal Statistical Society Series B, 73, 273-282.

436 Tsuda, S., Yoshida, T., Tsutsumi, M., Saito, K., 2015. Characteristics and verification of a
437 car-borne survey system for dose rates in air: KURAMA-II. J. Environ. Radioact. 139, 260-
438 265. doi: 10.1016/j.jenvrad.2014.02.028.
439
440 Wainwright, H.M., Seki, A., Mikami, S., Saito, K., 2018. Characterizing regional-scale
441 temporal evolution of air dose rates after the Fukushima Daiichi Nuclear Power Plant
442 accident. J. Environ. Radioact. 189, 213–220.
443
444 Yoshimura K, Saito K, Fujiwara K., 2017. Distribution of $^{137}$Cs on components in urban area
445 four years after the Fukushima Dai-ichi Nuclear Power Plant accident. J. Environ. Radioact.
446 178-179, 48-54.
447

448 **Figure captions**

449

450 **Fig 1.** Tendency of the air dose rate reduction for different ecological half-lives assumed in
451 the basis functions.

452

453 **Fig 2.** Examples of the least absolute shrinkage and selection operator (LASSO) analysis
454 results with the observed air dose rate.

455

456 **Fig 3.** The distribution of the number of basis functions for a) the fast-decay and b) the slow-
457 decay components in the two-component model.

458

459 **Fig 4.** The distribution of the number of basis functions in the one-component model.

460

461 **Fig 5.** The average profile of ecological half-lives for five land-use categories for pixels with
462 an initial air dose rate of more than 0.2 μSv/h.

463

464 **Fig. 6.** The difference in the decreasing tendency of air dose rates due to land use

465

466 **Fig. 7.** The average profile of ecological half-lives classified by the initial dose rate.

467

468 **Fig. 8.** The difference in the decreasing tendency of air dose rates due to the initial dose rate

469

**Table captions**

**Table 1** Information on the car-borne survey data used for the least absolute shrinkage and selection operator (LASSO) analysis. The pixels with more than 11 data in the 13 campaigns were selected for the analysis.

**Table 2** Ecological half-lives assumed in the basis functions for the least absolute shrinkage and selection operator (LASSO) analysis. The fifty half-lives were given between 0.1 y and 50 y corresponding to the ecological attenuation coefficients $\lambda_i$ to cover the tendencies of air dose rate attenuation evenly.

**Table 3** The number of pixels classified by land use and initial dose rate.

**Table 4** Proportion of the selected model in terms of the component number.

**Table 5** The sum of the average normalized coefficients of the basis functions for the periods less than 1 y and more than 1 y.

**Table 6** The average ecological half-lives for the periods less than 1y and more than 1 y.

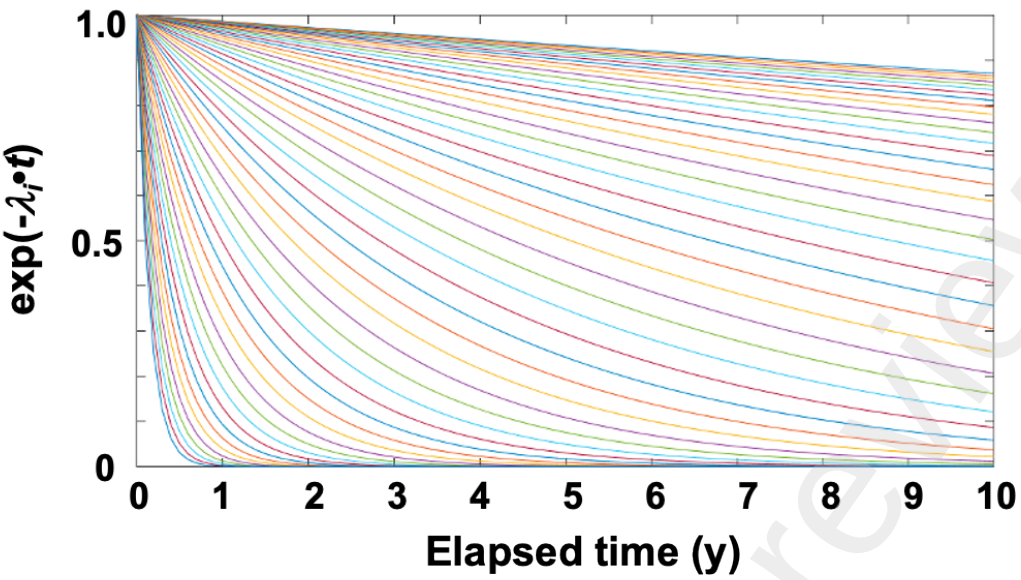


491

492 **Fig. 1.** Tendency of the air dose rate reduction for different ecological half-lives assumed in

493 the basis functions.

494

495

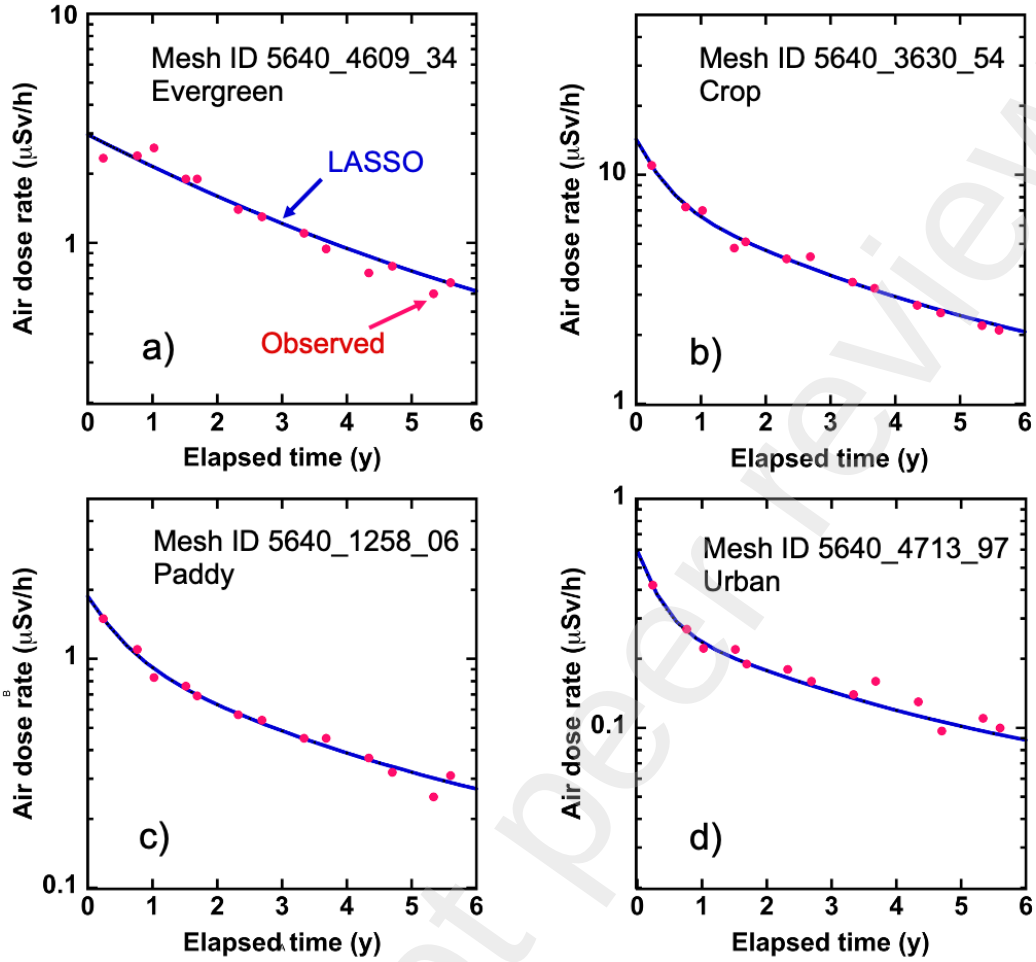


**Fig. 2.** Examples of the least absolute shrinkage and selection operator (LASSO) analysis results with the observed air dose rate.

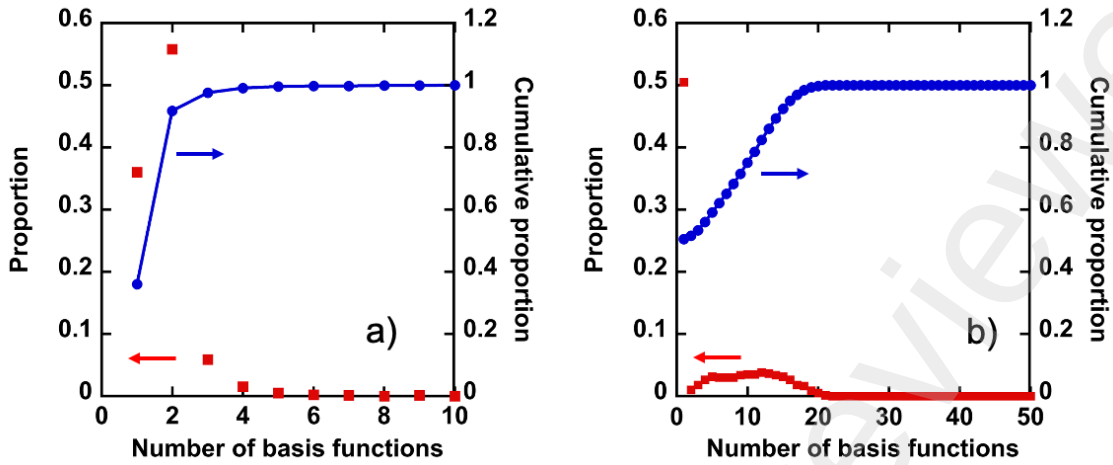


**Fig. 3.** The distribution of the number of basis functions for a) the fast-decay and b) the slow-decay components in the two-component model.

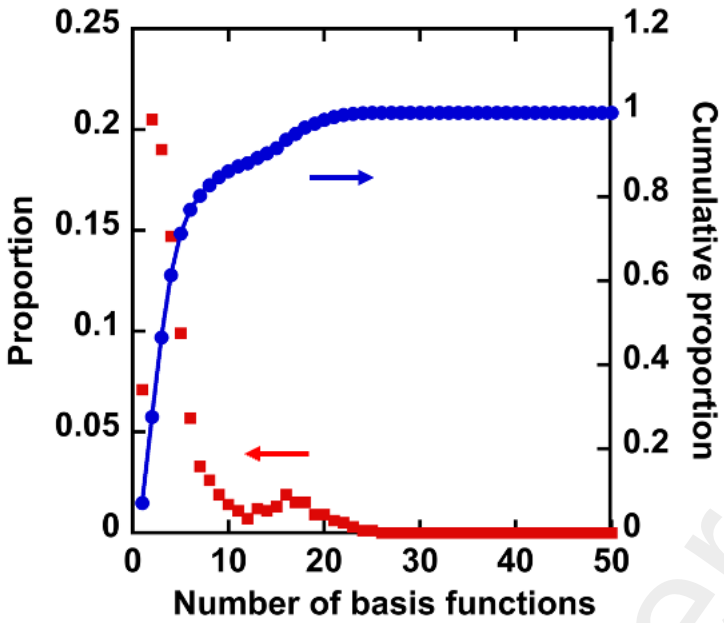


506

507 **Fig. 4.** The distribution of the number of basis functions in the one-component model.

508

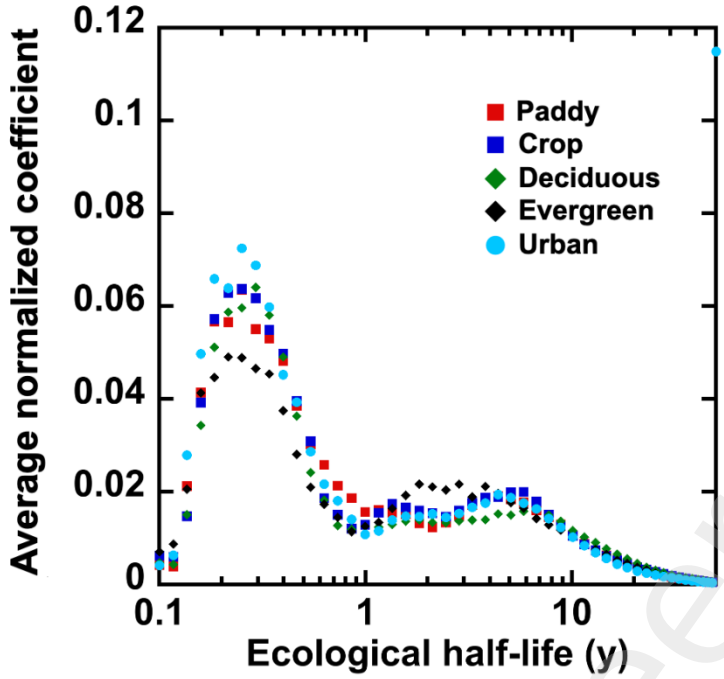


509

510 **Fig. 5.** The average profile of ecological half-lives for five land-use categories for pixels with

511 the initial air dose rate of more than 0.2 mSv/h.

512

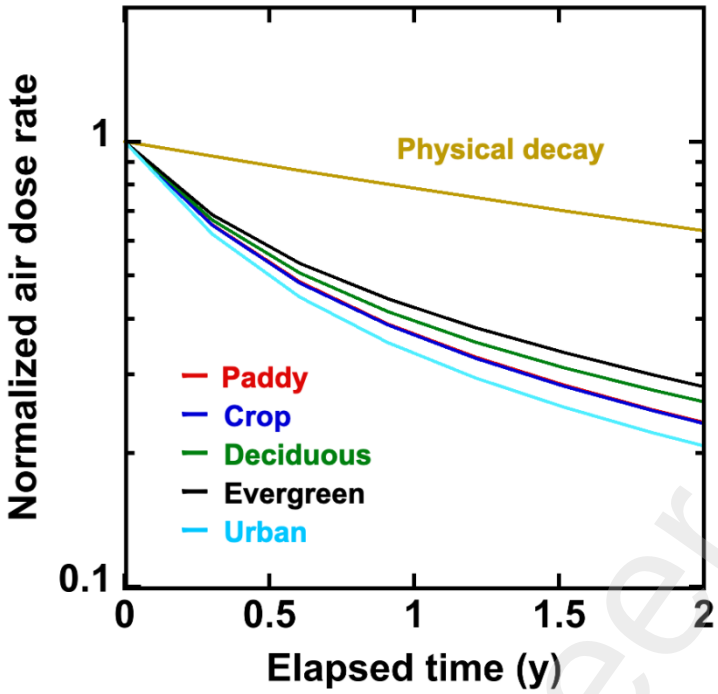


513

514 **Fig. 6.** The difference in the decreasing tendency of air dose rates due to land use.

515

516

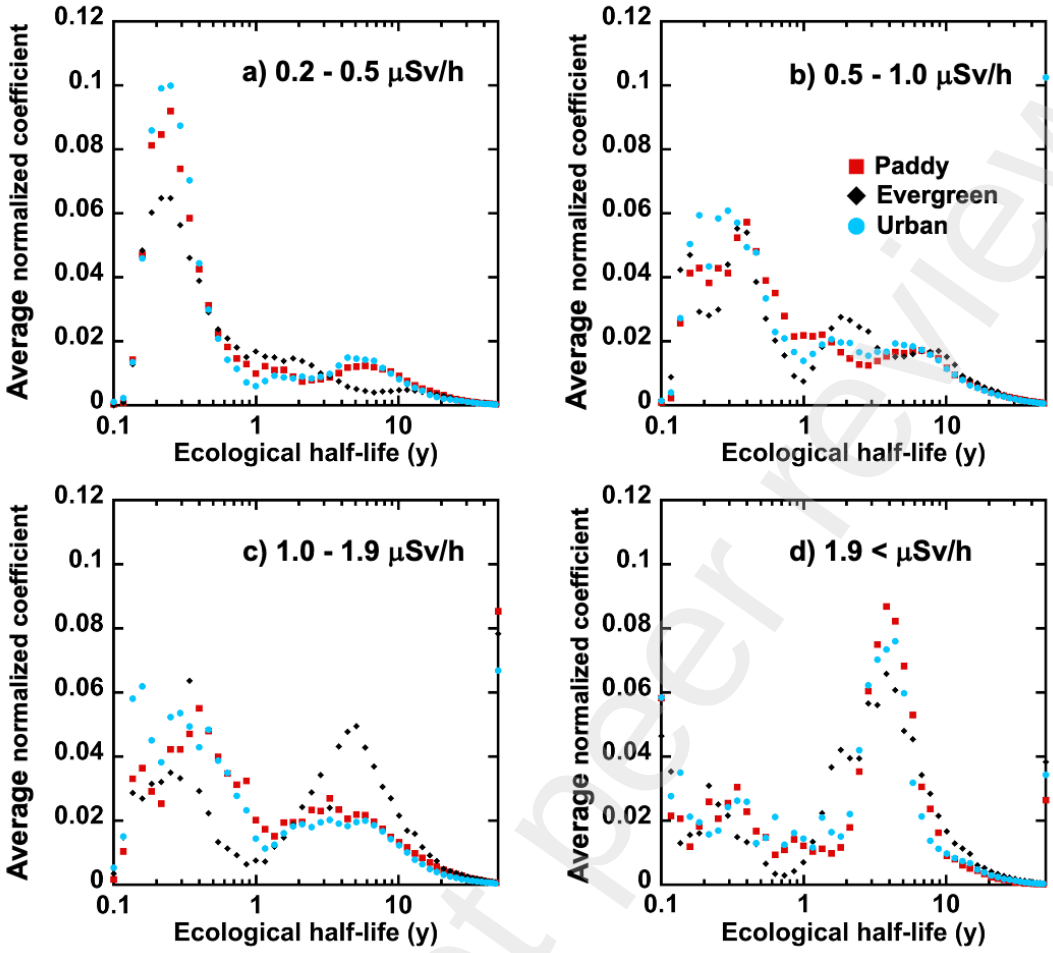


517

518 **Fig. 7.** The average profile of ecological half-lives classified by the initial dose rate.

519

520

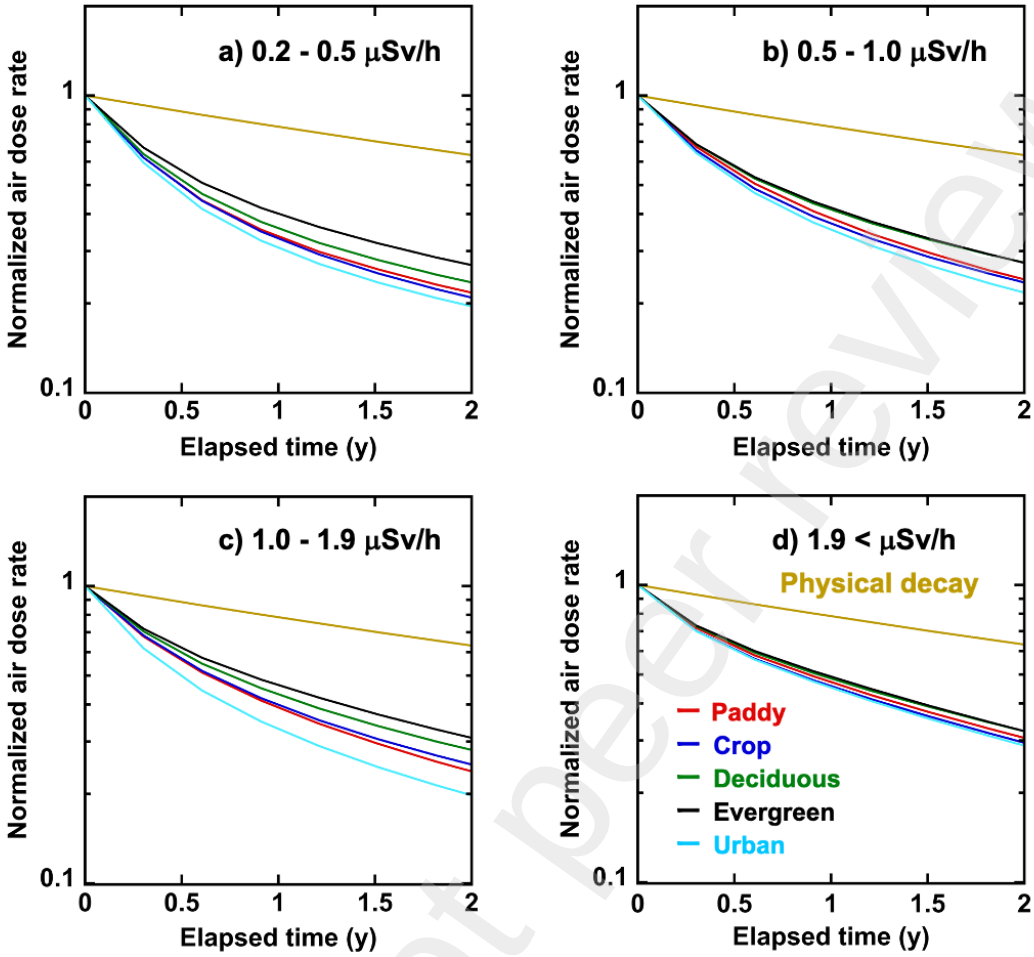


521

522 **Fig. 8.** The difference in the decreasing tendency of air dose rates due to the initial dose rate.

523

**Table 1**

Information on the car-borne survey data used for the least absolute shrinkage and selection operator (LASSO) analysis. The pixels with more than 11 data in the 13 campaigns were selected for the analysis from these data.

| Campaign No. | Duration (day/month/year) | Elapsed time after the accident (y) | Number of pixels |
|---|---|---|---|
| 1 | 6/6/2011 - 13/6/ 2011 | 0.24 | 45,273 |
| 2 | 5/12/2011 - 28/12/2011 | 0.76 | 36,355 |
| 3 | 13/3/2012 - 30/3/2012 | 1.02 | 38,741 |
| 4 | 20/8/2012 - 12/10/2012 | 1.51 | 132,380 |
| 5 | 5/11/2012 - 10/12/2012 | 1.69 | 89,385 |
| 6 | 12/6/2013 - 8/8/2013 | 2.32 | 129,666 |
| 7 | 5/11/2013 - 12/12/2013 | 2.69 | 119,522 |
| 8 | 23/6/2014 - 8/8/2014 | 3.34 | 102,473 |
| 9 | 4/11/2014 - 5/12/2014 | 3.68 | 102,881 |
| 10 | 29/6/2015 - 4/8/2015 | 4.34 | 100,235 |
| 11 | 2/11/2015 - 18/12/2015 | 4.70 | 89,849 |
| 12 | 27/6/2016 - 5/8/2016 | 5.34 | 100,854 |
| 13 | 31/10/2016 - 16/12/2016 | 5.69 | 86,255 |

**Table 2**

Ecological half-lives assumed in the basis functions for the least absolute shrinkage and selection operator (LASSO) analysis. The fifty half-lives were given between 0.1 y and 50 y corresponding to the ecological attenuation coefficients $l_i$ to cover the tendencies of air dose rate attenuation evenly.

| No. | Ecological half-life (y) | | | | | | | | | |
|---|---|---|---|---|---|---|---|---|---|---|
| | 1 | 2 | 3 | 4 | 5 | 6 | 7 | 8 | 9 | 10 |
| 0 | 0.10 | 0.12 | 0.14 | 0.16 | 0.18 | 0.22 | 0.25 | 0.29 | 0.34 | 0.40 |
| 10 | 0.46 | 0.54 | 0.63 | 0.73 | 0.85 | 0.99 | 1.15 | 1.34 | 1.56 | 1.81 |
| 20 | 2.11 | 2.44 | 2.83 | 3.28 | 3.80 | 4.39 | 5.07 | 5.84 | 6.71 | 7.70 |
| 30 | 8.82 | 10.1 | 11.5 | 13.0 | 14.7 | 16.5 | 18.5 | 20.7 | 23.0 | 25.4 |
| 40 | 27.9 | 30.4 | 33.0 | 35.6 | 38.2 | 40.8 | 43.3 | 45.6 | 47.9 | 50.0 |

**Table 3**

The number of pixels classified by land use and initial dose rate.

| Land use | Number of pixels | | | | | Total |
|---|---|---|---|---|---|---|
| | Initial air dose rate (mSv/h) | | | | | |
| | 0-0.2 | 0.2–05 | 0.5–1.0 | 1.0–1.9 | 1.9< | |
| Paddy | 865 | 2,188 | 1,712 | 670 | 300 | 5,735 |
| Crops | 507 | 1,487 | 1,001 | 658 | 338 | 3,991 |
| Deciduous forest | 428 | 2,051 | 1,076 | 552 | 411 | 4,518 |
| Evergreen forest | 265 | 914 | 346 | 168 | 232 | 1,925 |
| Urban | 582 | 1,860 | 1,673 | 885 | 172 | 5,172 |
| Total | 2,647 | 8,500 | 5,808 | 2,933 | 1,453 | 21,341 |

**Table 4**

Proportion of the selected model in terms of the component number.

| Land use | Proportion | | |
|---|---|---|---|
| | Number of components | | |
| | 1 | 2 | 3 |
| Paddy | 0.21 | 0.78 | 0.006 |
| Crops | 0.18 | 0.81 | 0.007 |
| Deciduous forest | 0.17 | 0.82 | 0.006 |
| Evergreen forest | 0.24 | 0.75 | 0.004 |
| Urban | 0.19 | 0.81 | 0.005 |
| Total | 0.19 | 0.8 | 0.006 |

**Table 5**

The sum of the average normalized coefficients of the basis functions for the periods less tha1 y and more than 1 y.

| Dose rate range (mSv/h) | Sum of normalized coefficients (-) | | | | | | | | | |
|---|---|---|---|---|---|---|---|---|---|---|
| | Paddy | | Crop | | Deciduous | | Evergreen | | Urban | |
| | < 1 y | 1 y < | < 1 y | 1 y < | < 1 y | 1 y < | < 1 y | 1 y < | < 1 y | 1 y < |
| 0.2 - 0.5 | 0.60 | 0.40 | 0.62 | 0.38 | 0.58 | 0.42 | 0.52 | 0.48 | 0.64 | 0.36 |
| 0.5 - 1.0 | 0.54 | 0.46 | 0.54 | 0.46 | 0.49 | 0.51 | 0.46 | 0.54 | 0.57 | 0.43 |
| 1.0 - 1.9 | 0.53 | 0.47 | 0.52 | 0.48 | 0.46 | 0.54 | 0.37 | 0.63 | 0.61 | 0.39 |
| 1.9 < | 0.33 | 0.67 | 0.32 | 0.68 | 0.31 | 0.69 | 0.27 | 0.73 | 0.36 | 0.64 |

**Table 6**

The average ecological half-lives for the periods less than 1y and more than 1 y.

| Dose rate range (mSv/h) | Average ecological half-live (y) | | | | | | | | | |
|---|---|---|---|---|---|---|---|---|---|---|
| | Paddy | | Crops | | Deciduous | | Evergreen | | Urban | |
| | < 1 y | 1 - 50 y | < 1 y | 1 - 50 y | < 1 y | 1 - 50 y | < 1 y | 1 - 50 y | < 1 y | 1 - 50 y |
| 0.2 - 0.5 | 0.32 | 7.4 | 0.34 | 6.7 | 0.33 | 7.2 | 0.35 | 6.6 | 0.30 | 7.0 |
| 0.5 - 1.0 | 0.40 | 7.1 | 0.34 | 7.4 | 0.35 | 8.9 | 0.35 | 6.9 | 0.36 | 6.7 |
| 1.0 - 1.9 | 0.42 | 6.9 | 0.39 | 8.0 | 0.38 | 8.4 | 0.32 | 7.1 | 0.36 | 6.6 |
| 1.9 < | 0.32 | 5.1 | 0.26 | 4.8 | 0.29 | 6.7 | 0.26 | 5.4 | 0.33 | 5.0 |